Colloids and Surfaces A 591 (2020) 124562

Contents lists available at ScienceDirect

Colloids and Surfaces A

journal homepage: www.elsevier.com/locate/colsurfa

Spreading and adhesion forces for water droplets on methylated glass surfaces

Yujin Sun[a,b,*], Yatao Li[a], Xianshu Dong[a], Xiangning Bu[c,d], Jaroslaw W. Drelich[b,*]

[a] College of Mining Engineering, Taiyuan University of Technology, Taiyuan, 030024, Shanxi, China
[b] Department of Materials Science and Engineering, Michigan Technological University, Houghton, MI, USA
[c] Key Laboratory of Coal Processing and Efficient Utilization (Ministry of Education), China University of Mining &Technology, Xuzhou, 221116, China
[d] School of Chemical Engineering and Technology, China University of Mining & Technology, Xuzhou, 221116, China

GRAPHICAL ABSTRACT

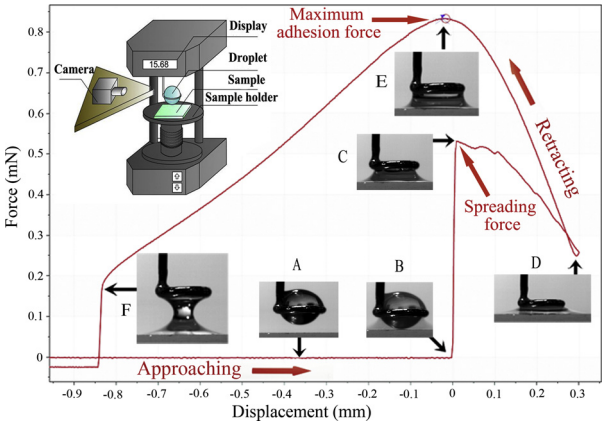

ARTICLE INFO

Keywords:
Adhesion force
Spreading force
Contact angle
Hydrophobicity
Wetting

ABSTRACT

Measurements of the spreading and capillary forces for liquids deposited on solid surfaces of varying surface chemistry and topography are a prerequisite to better understanding and quantification of the wetting mechanisms. In this study, glass slide surfaces were modified with trimethylchlorosilane to fabricate surfaces of varying hydrophobicity. Then, the forces of spreading and adhesion were measured between water droplets and glass surfaces using a high-sensitivity microelectronic balance. Integrated with a digital camera, the experimental set-up recorded forces and water droplet deformations during water droplet attachment, spreading, compression and retraction processes. It was confirmed that the spreading force increases with decreasing advancing contact angle for methylated glass, following a similar correlation as observed for smooth and rough polymers. However, the spreading force values for methylated glass were a few times lower than reported for polymers in spite of a similar roughness characteristic. It was also confirmed that the maximum adhesion force between water droplet and methylated glass increases with decreasing value of the most stable contact angle, a correlation that is similar to that reported for smooth polymers.

* Corresponding authors at College of Mining Engineering, Taiyuan University of Technology, Taiyuan, Shanxi, China
E-mail addresses: cumtsyj@163.com (Y. Sun), jwdrelic@mtu.edu (J.W. Drelich).

https://doi.org/10.1016/j.colsurfa.2020.124562
Received 20 November 2019; Received in revised form 30 January 2020; Accepted 6 February 2020
Available online 07 February 2020
0927-7757/

1. Introduction

Understanding the wetting characteristics of solid surfaces benefits a number of industrial operations and processes including wet processing of materials, froth flotation of minerals and plastics, wastepaper deinking, sewage treatment technologies, and fabrication of surfaces with designed functionality for antifouling, biomedical applications, microfluidics, and many others [1–7]. For instance, in the case of froth flotation, the stability of the intervening liquid film between a gas bubble and the particle surface depends on the adhesion strength between the aqueous phase and the mineral surface [8,9]. In addition, superhydrophobic surfaces with hydrophilic patterns are manufactured to realize microfluidic transportation [10], where spontaneous and directional pumpless transportation of oil droplets or gas bubbles are achieved under different fluids [11]. The designs of customized surfaces such as blood-repellent superhydrophobic surfaces [12], antifogging [13], self-regulating [14] and water harvesting surfaces [15] are driven by studying the factors that influence liquid – solid interactions.

Contact angles are widely used to quantify the wettability of natural and engineered solid surfaces [1,16]. Among several contact angle measurement techniques, the sessile drop method is the most commonly used due to its simplicity as well as the fact that both the advancing (θ_A) and the receding contact angles (θ_R) can be measured by changing the volume of a liquid droplet [17]. It is well documented that experimental contact angle values are influenced by the surface chemistry of the solid, including its heterogeneity pattern, surface geometry, and topographic features and their distribution [1,16]. Since surface characteristics in the solid-liquid contact area and at the perimeter of the liquid droplet base are rarely known in detail, interpretation of experimental contact angle values is almost never accomplished, contributing to a growing confusion about the meaning of measured contact angles and prompting misuses of contact angles [18].

In effort to understand relationships between experimental contact angles and solid surface characteristics, research attention shifted recently towards direct measurements of adhesion and capillary forces in systems involving liquids, especially when the contact angle can be quantified at different stages of spreading, adhesion and liquid separation. The most promising instrument for this research is a microbalance integrated with a CCD camera that is capable of measuring the adhesion directly between a liquid droplet and solid surfaces of different shape and topography and concurrently capturing images of a droplet during all stages of its attachment to solid (or liquid), spreading, and separation [19–22]. The correlations between adhesion forces and contact angles for solid surfaces of varying surface characteristics are not conclusive yet, although several useful observations were revealed in recent publications. For example, as expected, Liu et.al [20] confirmed a decrease in liquid droplet – solid adhesion force with increasing contact angle for gold surfaces modified with self-assembled monolayers of controllable wettability gradient. Samuel et.al [19] attempted to correlate apparent contact angles, including advancing and receding contact angles, measured independently using goniometry, with adhesion forces for water droplets in contact with 20 samples of different topography characteristics and found no correlation. Sun et al. [21,23] demonstrated experimentally that apparent advancing contact angles measured independently are nearly identical to advancing contact angles measured directly for droplets after their complete spreading on smooth polymers, during force measurements with a microbalance. These values were found to correlate well with recorded spreading forces. They also reported apparent receding contact angle values measured with goniometry that were nearly identical to the receding contact angle measured during droplet pull-off from polymeric surfaces. The receding contact angles correlated well with pull-off forces during droplet detachment from the smooth polymer surface whenever detachment of entire or nearly entire water droplets took place during separation. Such contact angle vs. force correlations, however, were not confirmed for polymeric patterns and in fact, are not expected for the majority of rough substrates. In the case of patterns/rough surfaces, the knowledge of triple-contact-line characteristics is necessary for correct interpretation of contact angles and forces [24].

Additionally, it was demonstrated earlier that contact angles measured for the most stable configuration of a liquid droplet in contact with a solid surface (reflected by the maximum adhesion force measured at a minimum in energy state for the liquid droplet – solid system under experimental conditions) can be characterized by the contact angle that is between the advancing and receding contact angle values, usually significantly closer to the receding contact angle than the advancing one [21,23]. The contact angle measured at the maximum adhesion force was referred to as the most stable contact angle.

In this study, spreading and adhesion forces were measured for water droplets in contact with methylated glass. Methylated glass was selected for this study because: (i) glass is a relatively smooth substrate that can be easily hydrophobized using silanes and produce surfaces having a broad range of hydrophobicity/hydrophilicity, and (ii) methylated glass is typically considered a heterogeneous surface (from a molecular to submicroscopic level), and heterogeneous surfaces were not yet used in force measurements using a microbalance. The primary objective here was to explore variations in spreading and adhesion forces for a water droplet in contact with heterogeneous surfaces of methylated glass and compare qualitatively the experimental values to similar forces recorded for polymers of similar wetting characteristics in terms of advancing and most stable contact angles.

2. Materials and methods

2.1. Materials

The glass slides used in this study were plain microscope slides purchased from Erie Scientific Company. All glass slides were washed multiple times to remove any organic and inorganic contaminants remaining on the surfaces of the original glass slides before their use and methylation. The cleaning process of the glass slides included the following steps: (a) washing with Micro-90 detergent solution; (b) rinsing with deionized water until all detergent was removed; (c) treating with acidic solution (2.5 v/v% H_2SO_4); (d) rinsing with deionized water; (e) treating with alkaline solution (2.5 w/v% NaOH); (f) rinsing with deionized water; (g) washing with absolute ethanol, and finally (h) drying in oven at 80 °C.

2.2. Methylation

Methylation was conducted according to the protocol reported earlier [25–27]. Analytical grade trimethylchlorosilane (TMCS) and cyclohexane (as solvent) obtained from Sigma-Aldrich were used for the methylation of glass slides to enhance their hydrophobicity, as per the following reaction:

$$-Si-OH + (CH_3)_3\,SiCl \rightarrow -Si-O-Si\,(CH_3)_3 + HCl$$

The chemicals were used as received without further purification. The concentration of TMCS in cyclohexane was 0.01 M. The degree of methylation was controlled by altering the methylation reaction time (0, 0.5, 1 and 2 h).

After methylation, glass slides were washed with cyclohexane and then absolute ethanol, dried in an oven and stored in a desiccator. The glass slides with increasing hydrophobicity were named glass A, B, C and D, respectively.

2.3. Contact angle measurements

The sessile drop method was used in measurements of advancing and receding contact angles for deionized water using the G10 Drop Shape Analysis system (Krüss GmbH, Germany) [17,28]. An average

value and standard deviation of at least 10 independent measurements are reported in this study.

2.4. Surface imaging

The MFP-3D Origin atomic force microscope (AFM, Asylum Research, Oxford Instruments, USA) was used in tapping mode operation for topographic imaging of the glass surfaces and determination of surface roughness under ambient atmospheric conditions. Three separate scans, each covering an area of 100 μm^2, were acquired for each of the samples at random locations to calculate the average value and standard deviation of root-mean-square (RMS) roughness parameter.

2.5. Adhesion force measurements

The forces of spreading, maximum adhesion and separation were measured for water droplets on glass slides using a high-sensitivity (± 1 μN/m) microelectronic mechanical balance system (Dataphysics DCAT 21, Germany) at room temperature of 22 °C–25 °C. HPLC water obtained from Sigma-Aldrich was used in all force measurements. A platinum/iridium ring holding an approximately 4 μL water droplet was connected to the balance. In this balance, a sample holder is immobilized on the upper side of a lift, which is driven by a computerized motor that has a variable velocity within a range of 0.7 μm/s to 8 mm/s. In this study, the sample holder was lifted upward at a preadjusted velocity of 0.03 mm/s as it approached the suspended water droplet. At the point of contact, the software senses the force of spreading between the water droplet and the sample surface. After the contact is made, the sample surface continues to move up to the compression distance (CD) pre-set by the user. The CD values selected for this study were 0, 0.1, 0.3 and 0.5 mm. After the CD value is reached, the solid surface retracts at the same velocity of 0.03 mm/s. The separation force is the largest just before the water droplet base retreats and the droplet pulls off the sample surface. The force versus displacement is recorded automatically by the software. In addition, a high-speed CCD camera is employed to record the spreading, compression and retraction stages as they occur. From captured images, the shape of the water droplet is analyzed and the contact angle is determined at each stage of contact between droplet and sample.

Fig. 1 shows a picture of the instrument (Fig. 1a), its schematic (Fig. 1b), and an image of a water droplet at the point of maximum adhesion detected during force measurements (Fig. 1c), on which the radius of droplet surface curvature and measured contact angle are marked. The contact angles on both sides of the droplet were measured and the average value is reported in this paper. More details on contact angle measurements are provided in our previous contribution [21].

Table 1
Advancing and receding water contact angles measured with goniometer, and RMS roughness measured with AFM for glass slides and polymers (Nylon = polyamide 6, PET = polyethylene terephthalate, EVA = ethylene vinyl acetate, PDMS = polydimethylsiloxane) [21].

Samples	θ_A /°	θ_R /°	RMS/nm
Glass slides – this study			
glass A	5 ± 2	< 5	7 ± 2
glass B	67 ± 2	33 ± 2	7 ± 3
glass C	74 ± 3	39 ± 3	8 ± 1
glass D	114 ± 3	51 ± 2	9 ± 1
Polymers – Sun et al.			
Nylon	63 ± 1	29 ± 1	11 ± 6
PET	77 ± 1	54 ± 1	4 ± 1
EVA	100 ± 2	77 ± 2	340 ± 200
PDMS	117 ± 2	78 ± 1	6 ± 4

3. Results and discussion

3.1. Wettability of samples

Table 1 summarizes the mean values ± standard deviation for advancing (θ_A) and receding (θ_R) contact angles measured for water droplets on glass surfaces using goniometry, and RMS roughness measured with AFM for glass slides and polymers. Examples of the droplet images during measurements of the advancing and receding contact angles are showed in Fig. 2. Glass A refers to a cleaned glass slide and glasses B to D refer to hydrophobized glass slides of increasing coverage with trimethylsilane functionality.

Iglauer et al. [29] reported water contact angles on a clean glass substrate in the range of 0-30°. They argued that the reported broad data for contact angles on glass substrate was caused by surface contamination. The advancing contact angle measured in this study for unmodified glass is about 5°, indicating that multiple cleaning of the glass can produce a surface with high hydrophilicity. However, such high sample cleanness is indeed short-lived in a regular laboratory environment and both organic contaminants and dust particles from surrounding air can deposit on glass slides in a matter of minutes.

Methylated glasses B and C are still categorized as hydrophilic surfaces, with advancing contact angles of about 67 and 74°, respectively. These values are consistent with contact angles reported in the literature when similar methylation protocol was used [30]. Glass D is hydrophobic with an advancing contact angle of about 114°, which matches the value reported by Rezayi et al., where the immersion time in TMCS solution (10 % v/v) was 30 min. [31].

As typically reported for methylated glass, the receding contact angles are significantly lower than advancing contact angles, resulting in a contact angle hysteresis (difference between θ_A and θ_R) from about 34–35° for glasses B and C to about 63° for glass D. Heterogeneity of hydrophilic glass surfaces coated with hydrophobic trimethylsilane

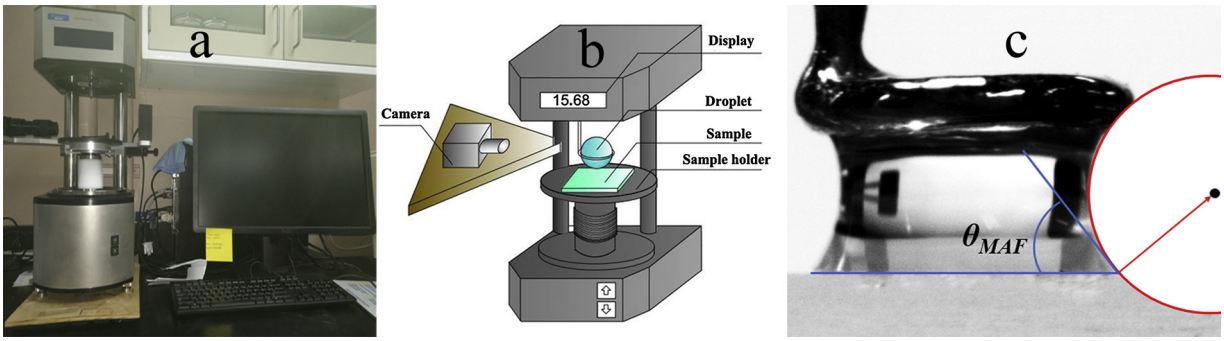

Fig. 1. a) Instrument used in this study; b) schematic of the instrument and its major components; and c) image of droplet at maximum adhesion configuration with marked surface curvature and measured contact angle.

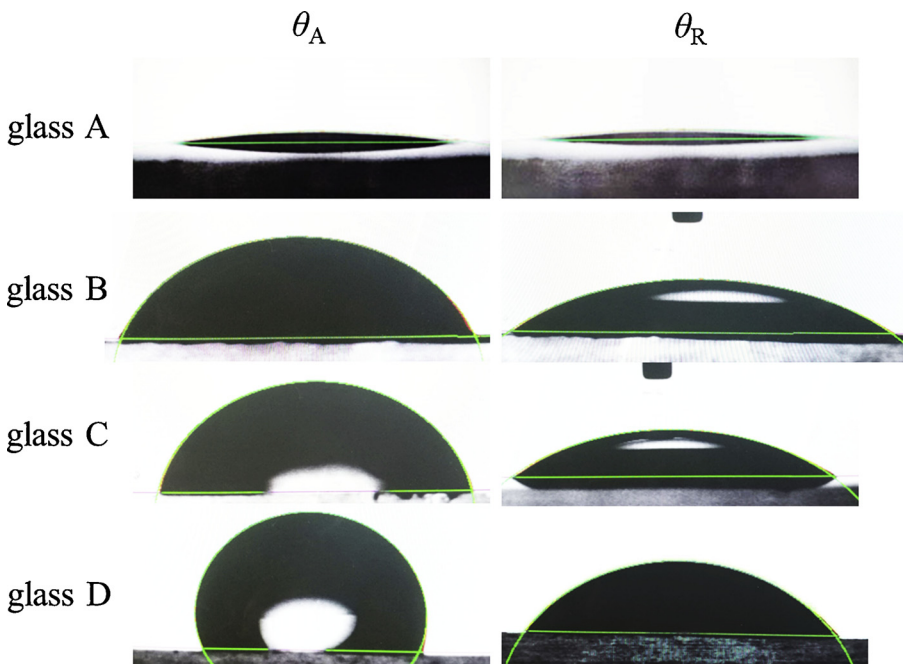

Fig. 2. Profiles of water droplets captured during the advancing and receding contact angle measurements for the glass A, B, C and D.

functionality is certainly a significant contributor to contact angle hysteresis. However, as discussed in a recent review [16], the sources of contact angle hysteresis go beyond commonly considered surface roughness and heterogeneity effects; these sources are not discussed in this contribution.

3.2. Surface topography

Topographic images of clean and methylated glass slides are shown in Fig. 3. The RMS roughness value determined for a clean glass slide (glass A) was 7 ± 2 nm (Table 1). Hydrophobization with trimethylsilane had very small effect on surface roughness, which increased to 9 ± 1 nm for glass D (Table 1). Therefore, the glass slides used in this study had high quality surfaces with nano-sized roughness of similar magnitude to three polymers used in the past (Table 1).

3.3. Force profile and key parameters

An example of the force vs. displacement curve is shown in Fig. 4. As the first step, the net force was zeroed to provide the baseline (A) during force measurements. The attachment of water droplet to the glass surface caused the droplet to spread, which is reflected in an attractive capillary force and rapid force value surge from point B to C. Point B marks the point of contact and zero displacement position. The force appearing at the turning point C is referred to as the spreading force [21], also called snap-in force in early publications. The contact angle measured at point C refers to advancing contact angle (θ_a), which is typically identical or close to the advancing contact angle measured with a goniometer (θ_A) [21] (as is also shown later). Spreading of the water droplet after its contact with the glass slide is so spontaneous that no other force value can be captured between points B and C, eliminating the possibility of tracking spreading kinetics. The time of the spreading process (from point B to C) was recorded to be below 0.3-0.4 s. Therefore, the spreading velocity of the water droplet on the glass surface exceeded the droplet approaching velocity.

Then, between points C and D, the droplet is compressed mechanically against the ring by the sample, which causes the force to decrease. The direction of movement of the stage is reversed at point D. As the result, the water droplet base is pinned and the droplet is then stretched until the maximum adhesion force point at E. The contact angle measured at point E corresponds to the contact angle for the most stable water droplet/solid surface configuration (θ_{MAF}) and was referred in our previous publication as the *most stable contact angle* [21].

Further stretching of water droplet after point E results in decreasing force values, the consequence of decreasing capillary force for a progressively stretched droplet. The droplet contact line continues to pin and then slide, reducing the droplet base diameter, and the radius of curvature increases as the result of increasing distance between the solid surface and ring. This process continues until separation at point F. The force measured at point F is often called pull-off force but corresponds to the separation force if the entire, or nearly entire, droplet can be removed from the sample surface. The separation is only observed for hydrophobic and nearly hydrophobic surfaces, and the contact angle measured at this point corresponds to the receding contact angle (θ_r) [21,23], which is typically close to the receding contact angle (θ_R) measured with a goniometer. Point F in Fig. 4 (and for other hydrophilic samples) describes the point of critical necking of the droplet, when the cohesive force between water molecules is lower than the attractive adhesion force between water and the glass slide. The necking ends in splitting the water volume into two droplets: one still sitting in the ring and another (smaller one) left on the sample surface. The volume of the droplet remaining on the solid surface can be calculated from a difference between the baseline force (zero) and the negative force shown in Fig. 4 after point F; this analysis is not exercised in this contribution. Whenever water-solid adhesion is stronger than water cohesion and the water droplet divides, the contact angle measured at point F does not necessarily correspond to θ_r and can have a value in between θ_r and $\theta_{MAF.}$ Since the meanings of both force and contact angle measured at point F are unclear for methylated glass samples, the pull-off force values are not reported in this contribution.

Table 2 provides a summary of experimental forces, droplet – solid contact diameter and contact angles for all four samples. Both the contact diameter and contact angles were measured from captured images. As expected, the spreading force decreased with decreasing hydrophilicity, from about 530 μN for the hydrophilic surface of cleaned glass with an advancing contact angle of about 16 degrees to about 40 μN for fully hydrophobized glass with an advancing contact angle of 114 degrees. The contact diameters after spreading also

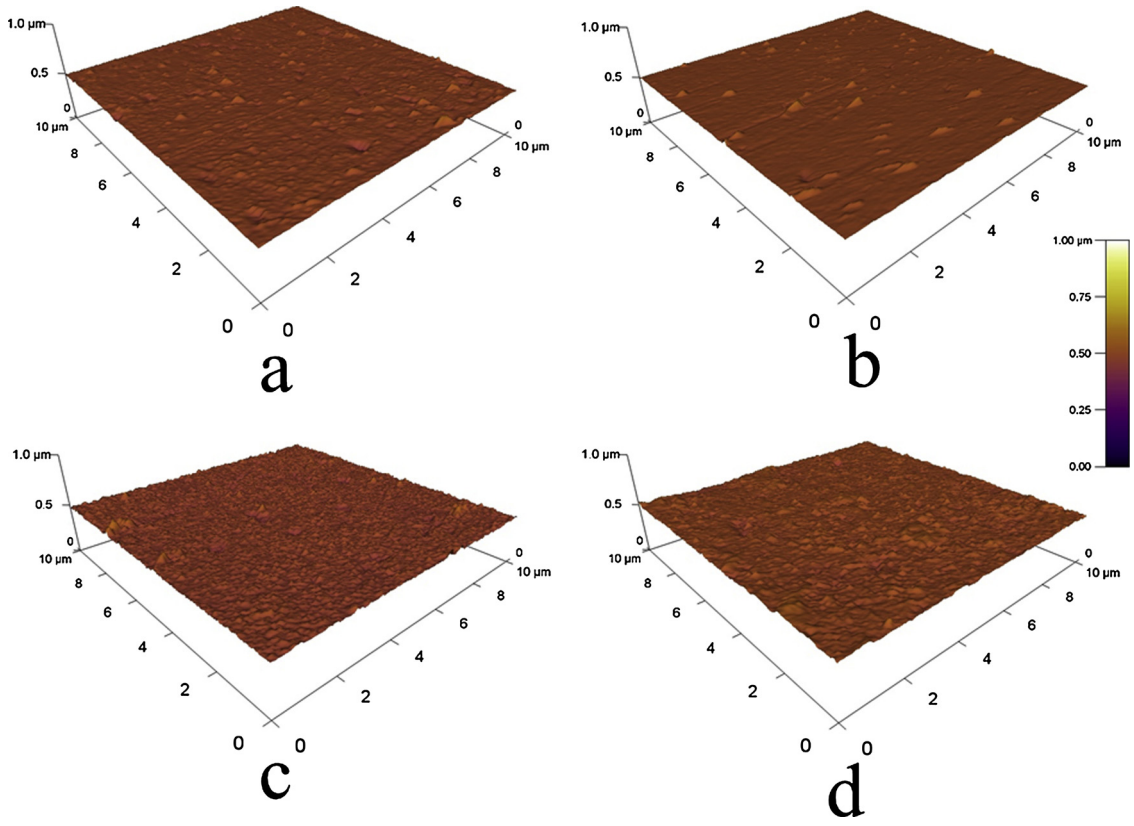

Fig. 3. 3D AFM topographic images of the glass A (a), B (b), C (c) and D (d) surfaces.

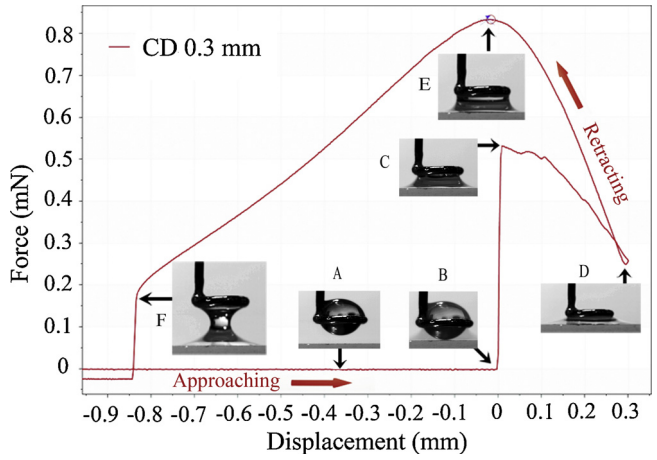

Fig. 4. A force profile recorded during a water droplet attachment, spreading, compression and retraction on a glass slide. The approaching and retracting velocities (V_a and V_r) were 0.03 mm/s. The insets A to F show shapes of water droplets at different stages of force measurements.

reflected changes in the affinity of water to glass surfaces and decrease from 3.24 mm for glass A to 1.24 mm for glass D. Also, maximum adhesion force values followed a very similar pattern with changes in surface hydrophilicity/hydrophobicity. The maximum adhesion force of about 740 μN for a cleaned glass slide with a most stable contact angle of about 15 degrees dropped to about 180 μN for fully silanized glass with a most stable contact angle of 83 degrees.

Both spreading and maximum adhesion forces can be calculated from droplet dimensions and measured contact angles by analyzing the capillary force, composed of two components: (i) the surface tension per unit length of the three-phase contact line and (ii) the Laplace pressure ΔP acting in the area of water droplet/solid adhesion, as per the following equation [32–35]:

$$F = 2\pi r\gamma \sin\theta - \pi r^2 \Delta P \quad (1)$$

where θ is the contact angle during the spreading (θ_a) or MAF configuration (θ_{MAF}), and the Laplace pressure:

$$\Delta P = \gamma\left(\frac{1}{D} - \frac{1}{R}\right) \quad (2)$$

where D and R are the principal radii of the spreading or adhered water droplet.

Table 2
Mean values and standard deviations for spreading (F_s) and maximum adhesion (F_{MAF}) forces, droplet base diameter ($2r$) and contact angles (θ) for experiments with compression distance of 0.1 mm.

Samples	Spreading			MAF		
	F_s [μN]	$2r$ [mm]	θ_a [deg]	F_{MAF} [μN]	$2r$ [mm]	θ_{MAF} [deg]
glass A	530 ± 16	3.24 ± 0.12	16 ± 3	741 ± 11	3.09 ± 0.03	15 ± 3
glass B	136 ± 41	2.52 ± 0.05	69 ± 4	587 ± 23	2.55 ± 0.02	36 ± 5
glass C	117 ± 8	2.12 ± 0.04	84 ± 3	426 ± 17	2.18 ± 0.04	49 ± 4
glass D	40 ± 2	1.24 ± 0.07	119 ± 6	182 ± 9	1.35 ± 0.04	83 ± 4

The deviation between experimental force values measured with the microbalance and calculated ones with Eq. (1) are typically within 5–10 %. Detailed validation of Eq. (1) was provided in our earlier publication [21] and will not be repeated here.

Finally, the advancing contact angles (θ_a) measured at the point of spreading force (F_s) can be compared to those measured with goniometry (θ_A) and listed in Table 1. All the θ_a (mean) values are larger by 2–11 degrees than θ_A values, which confirms that these values are close to advancing contact angles measured independently with the sessile-drop method. A similar range of differences was also reported in our earlier publication [21]. The difference is likely caused by small variations in measurement conditions. In the sessile-drop method [17], the droplet volume is progressively increased to volumes that are larger than the volume of the droplet used in force measurements. The effects of droplet size on both advancing and receding contact angles are well documented in the literature [28,36]. More importantly, the droplets are also allowed to spread freely over the sample surface in the sessile-drop method, whereas the droplet in force measurements is held hostage in the ring, adding extra tension on the droplet against its spreading.

3.4. The effect of compression distance on force curves

Figs. 5 and 6 show the force curves for tests conducted with varying compression distances. Changes in wettability of glass samples influenced the force curve slopes of compression (C to D), retraction (D to E), and dewetting (E to F), confirming the decreasing adhesion of water to glass samples of increasing hydrophobic component.

High affinity of water to a clean glass surface (glass A) was responsible for spontaneous spreading of a water droplet on this sample that disturbed the stability of a microbalance spring holding the ring with the water droplet and caused vibrations. These vibrations of force value are visible in the force curves after point C in Figs. 5a and 6 b and d (glass A). For other samples, no noticeable fluctuation of the force curve was observed, mainly because of decreasing affinity of water to hydrophobized glass samples, B to D. For example, the spreading force decreased nearly four and thirteen times for glass B and D as compared to the high spreading force of about 530 μN for an unmodified glass slide (Table 2).

Intuitively, the compression distance, changed during experimentation from CD = 0 to CD = 0.5 mm, should not affect the spreading force because the compression of water droplets takes place after droplet attachment and completion of spreading. However, in some instances increasing compression distance increased the experimental spreading force value (Fig. 7). For glasses A, B and C, the spreading force increased gradually with the increasing CD value, although there are significant differences in magnitude of this effect for different samples. The spreading force increased by nearly 100 % for glass B when the CD increased from 0 to 0.5 mm. This effect was reduced to about 10 % and 6 % for glasses C and A, respectively. As for the glass D, the spreading force remained practically constant regardless of CD.

We do not have a clear explanation for correlations in Fig. 7 and speculate that this effect relates to spreading time and resistance to water spreading caused by a ring holding the water droplet. By increasing the CD value, more time is provided for water droplet spreading to reach its final state. More importantly, by rising the sample closer to the holding ring, a tension from ring against spreading is reduced.

The experimental MAF values are plotted as a function of CD value in Fig. 8. By increasing the CD value, the attached water droplets were mechanically forced to spread to a larger base diameter ($2r$). As expected, the MAF value increases with increasing CD. As per Eq. (1), the adhesion force between the water droplet and the solid surface is related to the length of the three-phase contact line and it is also affected by the Laplace pressure component [21,37].

3.5. Correlation between spreading force and advancing contact angle

It is shown in Fig. 9a that the force that drives the water droplet to spread over the solid surface decreases monotonically with the increasing advancing contact angle, reflecting increasing hydrophobicity of the solid surface. As discussed earlier, with the exception of glass B, all other three samples show minor effect of CD on spreading force. For

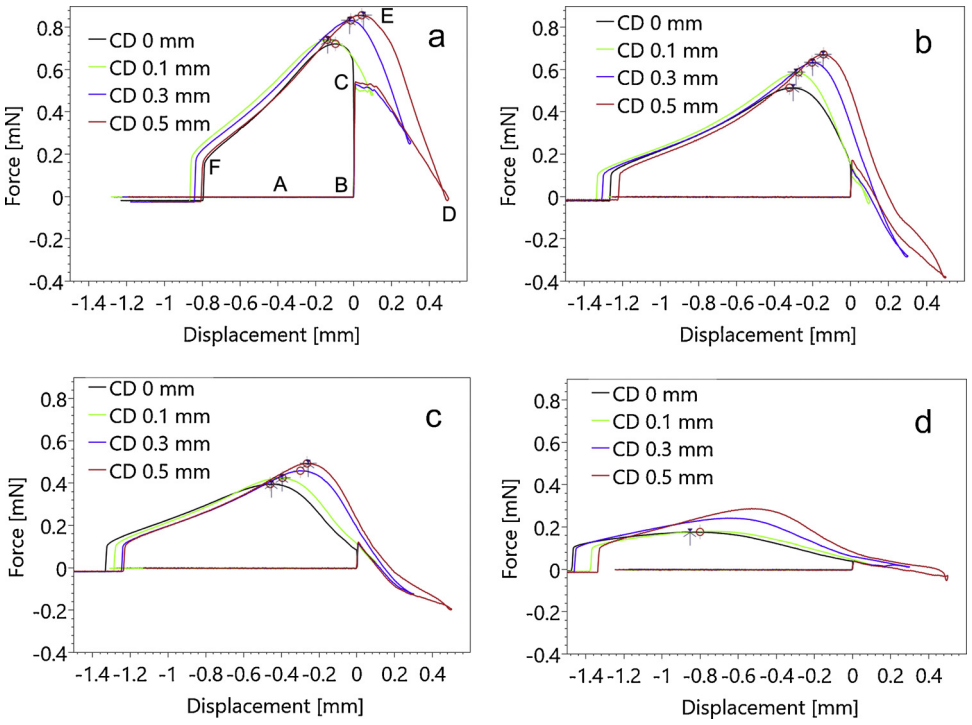

Fig. 5. Force profiles for water droplets on glass A (a), glass B (b), glass C (c) and glass D (d).

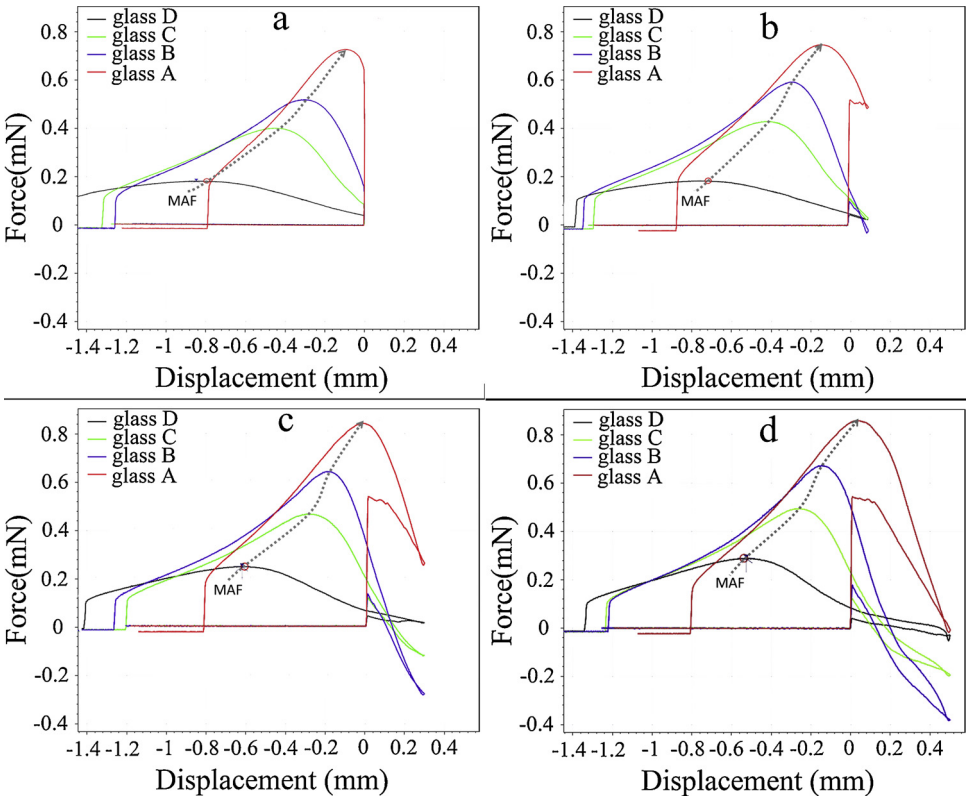

Fig. 6. The force curves for water droplets and glass surfaces with different CD of 0 mm (a), 0.1 mm (b), 0.3 mm (c) and 0.5 mm (d), respectively. The dotted lines are guides for the eye.

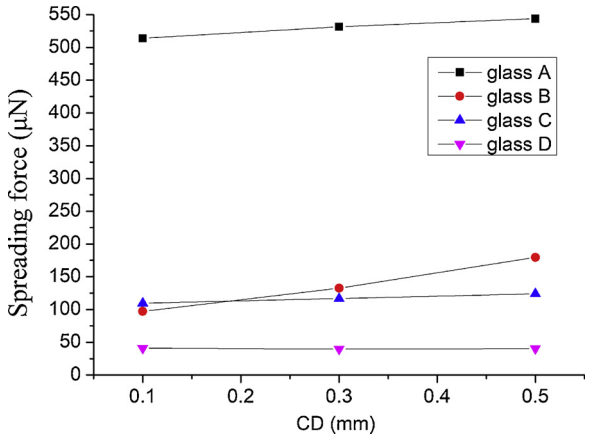

Fig. 7. Spreading force for the water droplets on glass A, B, C and D under different CD of 0.1, 0.3 and 0.5 mm.

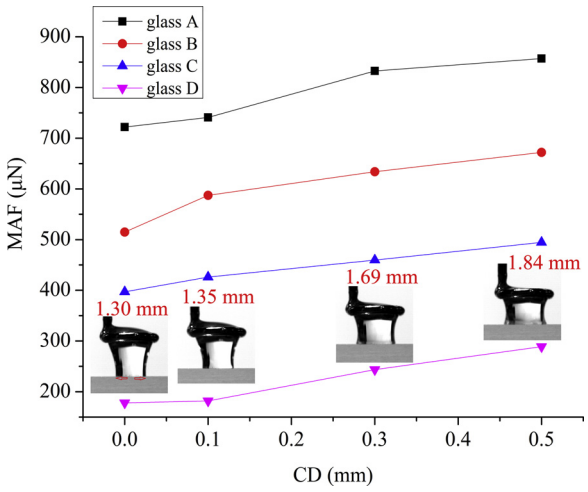

Fig. 8. Maximum adhesion force between water droplet and glass A, B, C and D under different CD value of 0.1, 0.3 and 0.5 mm. The insets present the droplet shape and the 2*r* (red number) for glass D at the MAF point. (For interpretation of the references to colour in this figure legend, the reader is referred to the web version of this article).

example, the spreading force decreased from about 544 μN to 40 μN (CD = 0.5) when the methylation time of the glass slides increased from 0 h to 2 h.

Fig. 9b presents the mean values of spreading forces from Fig. 9a and compares those to two other sets of data: for four different polymers published in our earlier publication [21] and several polymers of different roughness characteristics published by Samuel et al. [19] It should be noticed that the RMS roughness values were similar for glass slides used in this study and polymers used by Sun et al. [21], with exception of EVA (Table 1). Roughness of polymers was not quantified by Samuel et al. [19], although the majority of them could be considered as polymers with rough surfaces.

As shown in Fig. 9b, all three data sets show similar trends where the spreading force decreases with increasing advancing contact angle. Polynomial equations fitting the data are also included in Fig. 9b. It is interesting to note that although all three sets of data confirm the same trends, there are significant shifts in location of the trendlines. Surface roughness cannot explain it; both methylated glass and "smooth" polymers had nearly identical RMS values (Table 1). Further, Eq. (1) suggests that both radius of droplet base diameter and surface tension could be responsible for differences in spreading force. Droplet volume is controlled by the size of the ring. At least in our studies, the same ring was used allowing for only small, if any, variations in droplet volume and droplet base diameter after attachment and spreading on solid

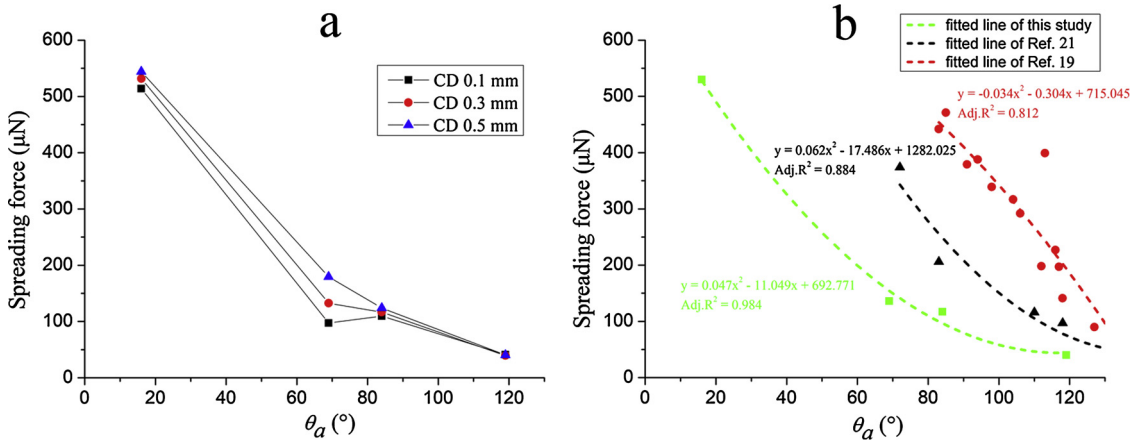

Fig. 9. a) Spreading force between water droplet and the glass surface with respect to the advancing contact angle; b) fit result between the spreading force and the advancing contact angle. Data source: ▲from ref.21 and ● from ref.19.

surfaces of particular wettability. Surface tension of water is sensitive to temperature and surface-active contaminants that can be picked up by water during experimentation from either the surrounding air or substrate. Temperature unfortunately was not controlled in any experimentation but variation of up to 4–5 degrees per set is not sufficient to explain differences in position of data sets in Fig. 9b. Contamination should not have any huge effect on data in Fig. 9b because each measurement is typically conducted with a fresh water droplet taken from a clean supply.

In conclusion, differences in location of data sets in Fig. 9b are puzzling but cannot be explained by roughness, at least for samples listed in Table 1. It could have some roots in differences in surface heterogeneity between samples. Methylated glass (or quartz) is known from its heterogeneity where hydrophilic substrate is non-uniformly covered with trimethylsilane functionalities [38]. We also speculate here that a variation in humidity level during experimentation could also affect the state of the glass surface. All these factors, unexplored in this study, deserve further investigation in a future but are beyond the scope of this contribution.

3.6. Correlation between maximum adhesion force and contact angle

The measurements of the most stable contact angle for liquids on solids of varying surface characteristics under actual laboratory conditions are extremely difficult with traditional goniometric methods [16]. The microbalance used in this study is capable of such measurements as demonstrated earlier [19,21]. The most stable contact angle values are measured at the point of maximum adhesion force, when the system is at the most (mechanically) stable configuration. Fig. 10 shows the correlation between the MAF and θ_{MAF}. The MAF values decrease monotonically with increasing θ_{MAF} for the glass samples. The data published in our earlier publication follow similar correlation. The closeness of the two sets of data confirms that small variations in droplet base radius and surface tension have rather small effect on correlations in Fig. 10, as well as those in Fig. 9b.

4. Conclusions

In this study, a sensitive microelectronic balance was employed to record the spreading and adhesion forces for water droplets on glass surfaces of varying surface coverage with trimethylsilane functionality. It was found that the spreading force increases with decreasing advancing contact angle but can also be sensitive to a compression distance value (distance over which the deposited droplet is compressed by the holding ring) set for the force measurements. In comparison to previously reported spreading forces for rough polymers, the spreading

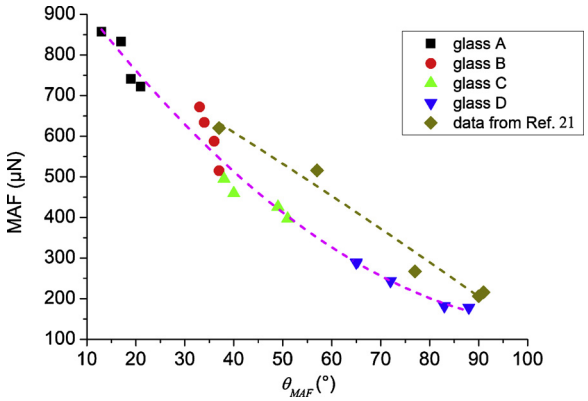

Fig. 10. MAF between water droplet and the glass surfaces with respect to most stable contact angle (θ_{MAF}). Data collected from ref.21 are also presented.

force values for methylated glasses with smooth surfaces were several times lower. In comparison to polymers with smooth surfaces, the spreading force values for methylated glass were still a few times lower. This finding suggests that the interpretation of spreading force as the function of globally measured apparent advancing contact angle might be over-simplification.

Further, it was demonstrated that the maximum adhesion force increases with decreasing value of the most stable contact angle (contact angle measured at the point of maximum adhesion). A trendline describing a correlation between maximum adhesion force and most stable contact angle for methylated glass samples was in close proximity to a similar trendline for smooth polymers.

This contribution sheds a new light on water – solid adhesion during and after droplet spreading. It provides new insights into challenges in designing the solid surface functionality and roughness with tailored liquid spreading and adhesion forces.

CRediT authorship contribution statement

Yujin Sun: Conceptualization, Methodology, Investigation, Writing - original draft, Resources. **Yatao Li:** Methodology, Investigation. **Xianshu Dong:** Supervision, Funding acquisition. **Xiangning Bu:** Writing - review & editing. **Jaroslaw W. Drelich:** Writing - review & editing, Project administration, Funding acquisition.

Declaration of Competing Interest

The authors declare that they have no known competing financial

interests or personal relationships that could have appeared to influence the work reported in this paper.

Acknowledgements

The financial support of this work from the National Natural Science Foundation of China (Nos. 51804213 and 51820105006) is gratefully acknowledged. This work was also supported by Science Foundation for Youths of Shanxi Province (201901D211039) and Scientific and Technological Innovation Programs of Higher Education Institutions in Shanxi (STIP). Financial support for purchasing atomic force microscope used in characterization of sample surface roughness at Michigan Technological University through NSF-CS-MRI grant #1725818 is appreciated as well.

The authors express appreciation to Mr. Donghui Wang for topographic imaging of the samples using the AFM instrument.

References

[1] J.W. Drelich, L. Boinovich, E. Chibowski, C. Della Volpe, L. Holysz, A. Marmur, S. Siboni, Contact angles: history of over 200 years of open questions, Surf. Innov. 8 (2019) 3–27.
[2] H. Teisala, H.J. Butt, Hierarchical structures for superhydrophobic and superoleophobic surfaces, Langmuir 35 (2018) 10689–10703.
[3] M. Nosonovsky, B. Bhushan, Superhydrophobic surfaces and emerging applications: non-adhesion, energy, green engineering, Curr. Opin. Colloid Interface Sci. 14 (2009) 270–280.
[4] Y. Sun, G. Xie, Y. Peng, Y. Chen, G. Ma, How does high intensity conditioning affect flotation performance? Int. J. Coal Prep. Util. 39 (2019) 302–316.
[5] H. Gao, Y. Liu, G. Wang, S. Li, Z. Han, L. Ren, Switchable wettability surface with chemical stability and antifouling properties for controllable oil–Water separation, Langmuir 35 (2019) 4498–4508.
[6] U.U. Ghosh, S. Nair, A. Das, R. Mukherjee, S. DasGupta, Replicating and resolving wetting and adhesion characteristics of a rose petal, Colloid Surf. A Physicochem. Eng. Asp. 561 (2019) 9–17.
[7] T. Darmanin, G. Godeau, F. Guittard, Superhydrophobic, superoleophobic and underwater superoleophobic conducting polymer films, Surf. Innov. 6 (2018) 181–204.
[8] J. Laskowski, Particle–bubble attachment in flotation, Miner. Sci. Eng 6 (1974) 223–235.
[9] J.W. Drelich, A. Marmur, Meaningful contact angles in flotation systems: critical analysis and recommendations, Surf. Innov. 6 (2018) 19–30.
[10] J. Liu, J. Song, G. Wang, F. Chen, S. Liu, X. Yang, X. Liu, Maskless hydrophilic patterning of the superhydrophobic aluminum surface by an atmospheric pressure microplasma jet for water adhesion controlling, ACS Appl. Mater. Inter. 10 (2018) 7497–7503.
[11] J. Song, Z. Liu, X. Wang, H. Liu, Y. Lu, X. Deng, I.P. Parkin, High-efficiency bubble transportation in an aqueous environment on a serial wedge-shaped wettability pattern, J. Mater. Chem. A 7 (2019) 13567–13576.
[12] V. Jokinen, E. Kankuri, S. Hoshian, S. Franssila, R.H. Ras, Superhydrophobic blood-repellent surfaces, Adv. Mater. 30 (2018) 1705104.
[13] K. Manabe, M. Matsuda, C. Nakamura, K. Takahashi, K.H. Kyung, S. Shiratori, Antifibrinogen, antireflective, antifogging surfaces with biocompatible nano-ordered hierarchical texture fabricated by layer-by-layer self-assembly, Chem. Mater. 29 (2017) 4745–4753.
[14] K.C. Manning, L.C. Majure, K. Rykaczewski, Hydration-state-modulated morphology, wetting and vapor permeation of the Opuntia surface, Surf. Innov. 7 (2019) 299–303.
[15] Y. Jiang, C. Machado, S. Savarirayan, N.A. Patankar, K.C. Park, Onset time of fog collection, Soft Matter 15 (2019) 6779–6783.
[16] J.W. Drelich, Contact angles: from past mistakes to new developments through liquid-solid adhesion measurements, Adv. Colloid Interface Sci. 267 (2019) 1–14.
[17] J.W. Drelich, Guidelines to measurements of reproducible contact angles using a sessile-drop technique, Surf. Innov. 1 (2013) 248–254.
[18] A. Marmur, C. Della Volpe, S. Siboni, A. Amirfazli, J.W. Drelich, Contact angles and wettability: towards common and accurate terminology, Surf. Innov. 5 (2017) 3–8.
[19] B. Samuel, H. Zhao, K.Y. Law, Study of wetting and adhesion interactions between water and various polymer and superhydrophobic surfaces, J. Phys. Chem. C 115 (2011) 14852–14861.
[20] J. Liu, B. Yu, B. Ma, X. Song, X. Cao, Z. Li, W. Yang, F. Zhou, Adhesion force spectroscopy of model surfaces with wettability gradient, Colloid Surf. A Physicochem. Eng. Asp. 380 (2011) 175–181.
[21] Y. Sun, Y. Jiang, C.H. Choi, G. Xie, Q. Liu, J.W. Drelich, Direct measurements of adhesion forces of water droplets on smooth and patterned polymers, Surf. Innov. 6 (2017) 93–105.
[22] G. Hurchalla, J.W. Drelich, Water repellency of hierarchically structured legs of water-walking striders and fire ants, Surf. Innov. 7 (2019) 184–193.
[23] Y. Sun, Y. Jiang, C.H. Choi, G. Xie, Q. Liu, J.W. Drelich, The most stable state of a droplet on anisotropic patterns: support for a missing link, Surf. Innov. 6 (3) (2018) 133–140.
[24] Y. Jiang, Y. Sun, J.W. Drelich, C.H. Choi, Spontaneous spreading of a droplet: the role of solid continuity and advancing contact angle, Langmuir 34 (2018) 4945–4951.
[25] P.T.L. Koh, F.P. Hao, L.K. Smith, T.T. Chau, W.J. Bruckard, The effect of particle shape and hydrophobicity in flotation, Int. J. Miner. Process. 93 (2009) 128–134.
[26] B. Johansson, R.J. Pugh, L. Alexandrova, Flotation de-inking studies using model hydrophobic particles and non-ionic dispersants, Colloid Surf. A Physicochem. Eng. Asp. 170 (2000) 217–230.
[27] O. Guven, M.S. Celik, J.W. Drelich, Flotation of methylated roughened glass particles and analysis of particle–bubble energy barrier, Miner. Eng. 79 (2015) 125–132.
[28] J.W. Drelich, J.D. Miller, R.J. Good, The effect of drop (bubble) size on advancing and receding contact angles for heterogeneous and rough solid surfaces as observed with sessile-drop and captive-bubble techniques, J. Colloid Interface Sci. 179 (1996) 37–50.
[29] S. Iglauer, A. Salamah, M. Sarmadivaleh, K. Liu, C. Phan, Contamination of silica surfaces: impact on water–CO2–quartz and glass contact angle measurements, Int. J. Greenh. Gas Con. 22 (2014) 325–328.
[30] M. Szkop, B. Kliszcz, A.A. Kasprzak, A simple and reproducible protocol of glass surface silanization for TIRF microscopy imaging, Anal. Biochem. 549 (2018) 119–123.
[31] T. Rezayi, M.H. Entezari, Achieving to a superhydrophobic glass with high transparency by a simple sol–gel-dip-coating method, Surf. Coat. Tech. 276 (2015) 557–564.
[32] H.J. Butt, M. Kappl, Normal capillary forces, Adv. Colloid Interface Sci. 146 (2009) 48–60.
[33] N. Ishida, N. Kinoshita, M. Miyahara, K. Higashitani, Effects of hydrophobizing methods of surfaces on the interaction in aqueous solutions, J. Colloid Interface Sci. 216 (1999) 387–393.
[34] W.A. Ducker, Z.G. Xu, J.N. Israelachvili, Measurements of hydrophobic and DLVO forces in bubble-surface interactions in aqueous-solutions, Langmuir 10 (1994) 3279–3289.
[35] L.X. Wang, D. Sharp, J. Masliyah, Z.H. Xu, Measurement of interactions between solid particles, liquid droplets, and/or gas bubbles in a liquid using an integrated thin film drainage apparatus, Langmuir 29 (2013) 3594–3603.
[36] J. Drelich, The effect of drop (bubble) size on contact angle at solid surfaces, J. Adhesion 63 (1997) 31–51.
[37] W. Xu, C.H. Choi, From sticky to slippery droplets: dynamics of contact line depinning on superhydrophobic surfaces, Phys. Rev. Lett. 109 (2012) 024504.
[38] J. Drelich, J.D. Miller, R.J. Good, The effect of drop (bubble) size on advancing and receding contact angles for heterogeneous and rough solid surfaces as observed with sessile-drop and captive-bubble techniques, J. Colloid Interf. Sci. 179 (1996) 37–50.